Pattern Recognition 45 (2012) 4300–4311

Contents lists available at SciVerse ScienceDirect

Pattern Recognition

journal homepage: www.elsevier.com/locate/pr

Improved direction estimation for Di Zenzo's multichannel image gradient operator

Lianghai Jin, Hong Liu *, Xiangyang Xu, Enmin Song

School of Computer Science and Technology, Huazhong University of Science and Technology, Wuhan 430074, China

ARTICLE INFO

Article history:
Received 11 May 2011
Received in revised form
25 May 2012
Accepted 7 June 2012
Available online 16 June 2012

Keywords:
Gradient
Multichannel image
Color edge detection

ABSTRACT

Gradient estimation is one of the most important tasks in image/video processing. For multichannel images, a classical and widely-used gradient method is Di Zenzo's gradient operator, which is based on the measure of squared local contrast variation of multichannel images. However, up to now, the indetermination of Di Zenzo's gradient direction has not been well solved, which results in errors occurring in most of the subsequent studies in which Di Zenzo's vector gradient is used. In this paper, this problem is solved thoroughly. Furthermore, the ranges of the values that the gradient angle should take in various cases are also analyzed. As an application in color image processing, a color version of Canny edge detector is implemented by introducing the new gradient estimator to the traditional grayscale image Canny operator. The experimental results indicate that the improved Di Zenzo's gradient operator is currently one of the best color gradient estimators and outperforms other state-of-the-art color image gradient methods. The improved multichannel gradient operator not only provides accurate gradient estimation but also is efficient and easy to implement.

1. Introduction

Gradient [1] has been widely used in image processing and computer vision in applications such as edge detection [2–6], image segmentation [7,8], corner detection [9], image fusion [10], image recognition [11], face detection [12], and object tracking [8,13]. For example, edge detection can be implemented by thresholding gradient magnitudes or by locating local maximum values of gradient magnitudes, and object tracking and recognition can be obtained by matching the gradient directions and at the same time using the gradient magnitudes of the pixels on the model object edges and candidate object edges.

The gradient associated with an image pixel is usually defined as a 2-D column vector, in which the vectorial angle denotes the direction of the largest growth of the image function. For grayscale images, numerous gradient estimators have been developed. However, for multichannel (multidimensional) images, which are usually described as vector fields [14], this issue has not received enough attention. From a general point of view, multidimensional gradient estimators can be divided into three major categories. The first type is characterized by a single estimate of the orientation and strength of an edge at a point [15]. The first such method is proposed by Robinson [16], who computed 24 directional derivatives (8 neighbors per color channel) and chose the one with the largest magnitude as the color gradient. Later, Ruzon and Tomasi [15] utilized a color distribution to represent a neighborhood and implemented color edge, junction, and corner detection. Their method first divides the current processing window in half with a line segment and computes a color distribution for each half, and then calculates the distance between the two distributions. This process is repeated using line segments with different orientations and the one with maximum strength is assumed as the orientation of the edge. Thus, the maximum strength and the direction normal to the corresponding orientation are regarded as the gradient magnitude and direction.

The second category of multichannel gradient methods is based on grayscale image gradient estimators. These operators calculate the gradient vectors for individual channels and then combine them to produce the final gradient vectors. According to different combination mechanisms, the resultant gradient can be the vector sum of the gradient vectors of individual channels, or the RMS (root mean square), or the maximum of the channel gradient magnitudes, or other mechanisms. However, these component-wise methods, as pointed out in [17], are unsatisfactory in some cases since in these methods the image channels do not actually cooperate with one another.

The third type of multidimensional gradient estimators is based on finding the maximum changes of image vectors. Among them, the simplest one is to define the resultant gradient as the vector in which the magnitude is the maximum of the Euclidean distances between the central pixel vector and its eight neighboring

* Corresponding author. Tel.: +86 27 87792212.
E-mail addresses: Lianghaijin@gmail.com (L. Jin), hongliu@hust.edu.cn (H. Liu).

0031-3203/$ - see front matter © 2012 Elsevier Ltd. All rights reserved.
http://dx.doi.org/10.1016/j.patcog.2012.06.003

pixel vectors and the direction is estimated from the direction of the maximum change [18]. Di Zenzo [17] proposed a classical and efficient multichannel gradient operator, which is based on the measure of squared local contrast variation of multichannel images. Scharcanski and Venetsanopoulos developed a local vector statistics based gradient method for color edge detection [19], in which they used the differences between the average color vectors of the samples inside the sub-windows in horizontal and vertical directions to estimate the maximum variation of a color image in each pixel position.

More recently, Nezhadarya and Ward proposed a new color image gradient operator [20]. This method first applies highpass and lowpass vector operators in an appropriate manner in both horizontal and vertical directions, where the highpass and lowpass operators are respectively used as vector difference estimate and noise smoothing. Then, an aggregation operator is performed on each direction to find the corresponding partial derivative.

Among these multidimensional gradient estimators mentioned above, perhaps the most classical and widely-used one is Di Zenzo's multichannel gradient operator [17]. However, Di Zenzo did not solve the problem of indetermination of the gradient direction. Although some researchers [21,22] have made further studies on Di Zenzo's vector gradient, to date this problem has not been well solved, which results in errors occurring in most of the later studies (see Section 2) in which Di Zenzo's vector gradient is referenced. This paper will solve this problem thoroughly and at the same time analyze the gradient angle ranges in various cases.

As an application in image processing, we apply the new multichannel gradient operator to color image edge detection, since gradient is closely related to edge detection and image segmentation. In color images, edges can be defined as meaningful discontinuities of image functions in vector fields [23,24]. Color edge detection techniques [23–27] can be roughly divided into two classes: monochromatic-based techniques that first detect edges in individual color channels separately and then combine the component results to be the color edges, and vector-valued techniques that treat color pixels as color vectors in a vector space to detect the abrupt changes. Vector approaches are generally preferred to component-wise techniques owing to the vector nature of color images and the strong spectral correlation that exists between color channels. Vector approaches mainly include the first- [17] and second- [21,22] order derivative methods which are based on color vector gradients, the directional vectors based difference methods (or called directional operators) [19], the methods based on vector order statistics [28,29], the difference vector operators [23,25], and other methods such as morphological gradient approaches [30], vector entropy methods [31,32], density estimation methods [33,34], and methods based on physics models [35] and principal axis analysis and moment-preserving [36].

The remainder of this paper is organized as follows. In Section 2, Di Zenzo's vector gradient and the related work are reviewed, and the proposed mechanism for solving the ambiguity in Di Zenzo's gradient angle is described in detail. Section 3 gives an application for color edge detection by applying the new gradient operator to the traditional grayscale image Canny operator. Finally, conclusions are drawn in Section 4.

2. Di Zenzo's gradient operator and the proposed method

In this section, we first briefly introduce Di Zenzo's multidimensional gradient method and the related studies, and analyze the existing problem in Di Zenzo's gradient operator and its variations. Then, we give the solution which is described by a theorem to the existing problem. The proof of the theorem is presented in Appendix A.

2.1. Di Zenzo's gradient operator

Let an m-band image be represented by the function $f:R^2\rightarrow R^m$ that maps a point (x,y) in R^2 to an m-vector $(f_1(x,y),f_2(x,y),\ldots,f_m(x,y))^T$ in R^m. Obviously, this definition includes grayscale images and color images as two special cases of $m=1$ and $m=3$.

Di Zenzo's gradient operator is described as follows. Consider the square of the variation of a multichannel image $f(x,y)$ at position $P(x,y)$ in direction θ:

$$\begin{aligned} df^2 &= \left|\left|f(x+\varepsilon\cos\theta,y+\varepsilon\sin\theta)-f(x,y)\right|\right|_2^2 \\ &\approx \sum_{i=1}^{m}\left(\frac{\partial f_i}{\partial x}\varepsilon\cos\theta+\frac{\partial f_i}{\partial y}\varepsilon\sin\theta\right)^2 \\ &= \varepsilon^2\left(\cos^2\theta\sum_{i=1}^{m}\left|\frac{\partial f_i}{\partial x}\right|^2+\sin^2\theta\sum_{i=1}^{m}\left|\frac{\partial f_i}{\partial y}\right|^2+2\cos\theta\ \sin\theta\sum_{i=1}^{m}\frac{\partial f_i}{\partial x}\frac{\partial f_i}{\partial y}\right) \end{aligned} \tag{1}$$

So, the rate of change of the image at position (x,y) in any direction θ, $f(\theta)$, is:

$$\begin{aligned} f(\theta) &= \cos^2\theta\sum_{i=1}^{m}\left|\frac{\partial f_i}{\partial x}\right|^2+\sin^2\theta\sum_{i=1}^{m}\left|\frac{\partial f_i}{\partial y}\right|^2+2\cos\theta\sin\theta\sum_{i=1}^{m}\frac{\partial f_i}{\partial x}\frac{\partial f_i}{\partial y} \\ &\triangleq E\cos^2\theta+2F\cos\theta\sin\theta+G\sin^2\theta, \end{aligned} \tag{2}$$

where

$$E=\sum_{i=1}^{m}\left|\frac{\partial f_i}{\partial x}\right|^2,\quad F=\sum_{i=1}^{m}\frac{\partial f_i}{\partial x}\frac{\partial f_i}{\partial y},\quad G=\sum_{i=1}^{m}\left|\frac{\partial f_i}{\partial y}\right|^2 \tag{3}$$

Then, the gradient direction is defined as the value $\theta_{\max}$ that maximizes $f(\theta)$:

$$\theta_{\max}=\frac{1}{2}\left(\arctan\frac{2F}{E-G}+k\pi\right) \tag{4}$$

Thus, $f(\theta_{\max})$ is the magnitude of the vector gradient. Obviously, there is an $\pi/2$ ambiguity in gradient direction $\theta_{\max}$.

Using tensor notations, Di Zenzo used the following equations to express the parameters E, F, and G in the above gradient equations. Take *RGB*-color images as an example and let r, g, b denote the unit vectors associated with the R, G, B color axes, respectively. The first partial derivatives can be written as

$$u=\frac{\partial R}{\partial x}r+\frac{\partial G}{\partial x}g+\frac{\partial B}{\partial x}b, \tag{5}$$

$$v=\frac{\partial R}{\partial y}r+\frac{\partial G}{\partial y}g+\frac{\partial B}{\partial y}b, \tag{6}$$

where R, G, and B are the color components in the r, g, b basis. Then, the parameters E, F, and G can be written in the form of vector inner products as follows:

$$E=u\times u,\quad F=u\times v,\quad G=v\times v \tag{7}$$

2.2. Related studies

Since Di Zenzo's vector gradient is effective, easy to implement, and performs fast, it has been widely accepted by researchers and applied in many color image and video processing tasks. After Di Zenzo proposed the gradient operator, some researchers have made further studies. One of representative improvements is Cumani's work [21]. Cumani extended Di Zenzo's gradient operator to the second derivative for color edge detection: the second directional derivative operator.

Let the unit vector $n=(n_1,n_2)=(\cos\theta,\sin\theta)$ represent any direction θ. Then, Eq. (2), which is called the squared contrast function by Cumani and denoted as $S(P,n)$, can be written as

$$S(P,n)=En_1^2+2Fn_1n_2+Gn_2^2 \tag{8}$$

The extreme values of $S(P,\boldsymbol{n})$ coincide with the eigenvalues of 2×2 matrix $A=\begin{pmatrix}E & F\\ F & G\end{pmatrix}$ and are attained when n is the corresponding eigenvector [37]. The extreme values $\lambda_\pm$ and the corresponding eigenvectors $n_\pm$ are given by

$$\lambda_\pm=\tfrac{1}{2}((E+G)\pm\sqrt{(E-G)^2+(2F)^2}), \tag{9}$$

$$n_\pm=(\cos\theta_\pm,\sin\theta_\pm) \tag{10}$$

where

$$\theta_+=\begin{cases}\text{Undefined}, & (E-G)^2+F^2=0\\ \frac{\pi}{4}+k\pi, & E=G \text{ and } F>0\\ -\frac{\pi}{4}+k\pi, & E=G \text{ and } F<0\\ \frac{1}{2}\arctan\frac{2F}{E-G}+k\pi, & \text{Otherwise}\end{cases}, \tag{11}$$

$$\theta_-=\theta_++\frac{\pi}{2} \tag{12}$$

It should be mentioned that most of the researchers take θ_+ as the vector gradient direction [21,23–26,38]. In fact, it is not always correct because in many cases θ_+ is not the gradient direction but θ_- is, as can be seen in Section 2.3.

A point P is considered as a possible edge point only when the first directional derivative $D_S(P,n)$ of the squared contrast function $S(P,n)$ in gradient direction n_+ is equal to zero. The directional derivative $D_S(P,n_+)$ can be written as

$$D_S(P,n_+)=\nabla S\cdot n_+=E_xn_1^3+(2F_x+E_y)n_1^2n_2+(G_x+2F_y)n_1n_2^2+G_yn_2^3 \tag{13}$$

Finally, localization of edge map can be obtained by zero-crossing detection, taking into account the sign changes of $D_S(P,n_+)$ in the gradient direction n_+. However, the sign of $D_S(P,n_+)$ is, until now, not uniquely defined. The definition of n_+ of the eigenvector of a matrix results in the fact that it is not certain whether n_+ or $(-n_+)$ is the sought-after vector. Since n_+ cubically rises in $D_S(P,n_+)$, $D_S(P,n_+)$ is directly dependent on the sign of n_+. To try to solve this problem, Cumani proposed the utilization of a quite heavy sub-pixel technique using bilinear interpolation method. Alshatti and Lambert [22] proposed a modification of Cumani's technique. Since λ_+ is an eigenvalue of the matrix A, the associated eigenvector n_+ can be directly determined. Thereby the complex approximation in the sub-pixel domain, as suggested by Cumani, is avoided.

2.3. Solution to the indetermination of Di Zenzo's gradient direction

As stated in Sections 2.1 and 2.2, the problem of ambiguity in Di Zenzo's gradient direction, to date, has not well solved. By carefully analyzing the property of Di Zenzo's vector gradient estimator, we obtain a clear solution to this problem. Furthermore, we also analyze the gradient angle ranges in various cases. For simplicity, a theorem is given below to describe our conclusion and the proof of the theorem is presented in Appendix A.

Table 1
A comparison between the gradient angles of the original Di Zenzo's gradient operator and the proposed improvement for different E, F, G values.

F	$E-G$	Di Zenzo's gradient angle	Proposed gradient angle
$F\geq 0$	$E\geq G$	$[k\pi, k\pi+\pi/4]$	$[k\pi, k\pi+\pi/4]$
$F\geq 0$	$E<G$	$[k\pi-\pi/4, k\pi]$	$[k\pi+\pi/4, k\pi+\pi/2]$
$F<0$	$E\geq G$	$[k\pi-\pi/4, k\pi]$	$[k\pi-\pi/4, k\pi]$
$F<0$	$E<G$	$[k\pi, k\pi+\pi/4]$	$[k\pi-\pi/2, k\pi-\pi/4]$
$F=0$	$E=G$	Undefined	Undefined

Theorem 1. For Di Zenzo's vector gradient operator, the gradient magnitude $f_{\max}$ and the gradient direction angle $\theta_{\max}$ are

$$f_{\max}=\tfrac{1}{2}\left((E+G)+\sqrt{(E-G)^2+(2F)^2}\right), \tag{14}$$

$$\theta_{\max}=\begin{cases}\text{sgn}(F)\arcsin\left(\frac{f_{\max}-E}{2f_{\max}-E-G}\right)^{1/2}+k\pi, & (E-G)^2+F^2\neq 0\\ \text{Undefined}, & (E-G)^2+F^2=0\end{cases}, \tag{15}$$

where the parameters E, F, and G are defined in Eq. (3), and sgn$(\bullet)$ is a sign function:

$$\text{sgn}(F)=\begin{cases}1, & F\geq 0\\ -1, & F<0\end{cases}$$

Furthermore, the gradient angle $\theta_{\max}$ satisfies the following constraints:

$$\theta_{\max}\in k\pi+\begin{cases}[0,\ \pi/4], & F\geq 0 \text{ and } E-G\geq 0\\ [\pi/4,\ \pi/2], & F\geq 0 \text{ and } E-G<0\\ [-\pi/2,-\pi/4], & F<0 \text{ and } E-G<0\\ [-\pi/4,\ 0], & F<0 \text{ and } E-G\geq 0\end{cases} \tag{16}$$

About the above theorem, we give a brief explanation. In this theorem, there is an π ambiguity in the gradient direction. It is to say, the gradient direction can point to the direction of the largest growth of the image function (positive direction) or its opposite direction (negative direction). This problem cannot be solved in multichannel image processing due to the vector nature of multichannel images. Unlike grayscale images where we can use gray values to determine whether the change from one pixel to another is positive or negative, in multichannel images there does not exist an unique method to sort and compare two multichannel vectors and to further determine the polarity of a change in multichannel images. In addition, this indetermination of the positive and negative of color image gradient directions has no influence on color edge detection methods which are based on the first- and second derivatives. Because both types of methods use the gradient magnitudes associated with two neighboring positions of the current pixel along the gradient direction to detect the local maximum and zero-crossing.

According to the theorem, we can see that it is not always correct in Di Zenzo's multichannel gradient operator choosing θ_+ given by Eq. (11) as the gradient direction, which are used by many studies [21,23–26,38]. For example, when $F\geq 0$ *and* $E-G<0$, $\theta_+\in[k\pi-\pi/4,k\pi]$ according to Eq. (11), whereas our result is $\theta_{\max}\in[k\pi+\pi/4,\ k\pi+\pi/2]$; and when $F<0$ *and* $E-G<0$, $\theta_+\in[k\pi,\ k\pi+\pi/4]$, whereas our result is $\theta_{\max}\in[k\pi-\pi/2,\ k\pi-\pi/4]$. The ranges of the values that the gradient angle should take in both the original Di Zenzo's gradient operator and the proposed improvement are summarized in Table 1.

3. Application in color edge detection

As mentioned in the introductory section, gradient is closely related to edge detection and image segmentation. So, in this

section, we apply the proposed multichannel gradient operator to color image edge detection. For edge detection, perhaps the best method to evaluate the accuracy of image gradients is Canny edge detector [2]. Because in Canny operator, both gradient magnitudes and directions are used to implement non-maximal suppression, which is the key step and significantly affects the performance of the edge operator. The traditional Canny operator is mainly used for grayscale images. By replacing the gradients of grayscale images in the traditional Canny operator with color image gradients, we can obtain various color versions of Canny edge detector. To evaluate the performance of the proposed multidimensional gradient estimator (**Proposed**), other state-of-the-art color image gradient methods are chosen for comparison. These rival color gradient operators include the original Di Zenzo's gradient operator (**Di Zenzo**) [17], Scharcanski and Venetsanopoulos' gradient estimator (**Scharcanski)** [19], **RCMG-Median–Mean** operator (note that RCMG-Median–Mean operator is the best gradient estimator among its gradient family according to the original paper) [20], and Ruzon and Tomasi's **Compass** operator [15]. In addition, to demonstrate the superiority of color vector gradient estimators against grayscale image gradient methods in color edge detection, we convert each color test image to a luminance image and use the gradients of the luminance image to represent the color image gradients (**Luminance-based gradient**). Note that in Di Zenzo's gradient operator, the gradient direction takes θ_+ denoted by Eq. (11), as most of the related studies do. In addition, due to the indetermination of polarities of vector changes (positive or negative) in multichannel images, we limit the directions of the color vector gradients produced by Di Zenzo's method and our improvement to major values $[-\pi/2, \pi/2]$.

For a fair comparison, we only use various gradient algorithms to compute the gradients of each color image (including magnitudes and direction angles). The resultant edge maps are obtained by the same Canny edge detector with different gradient calculations.

3.1. Synthetic images

Edge detection systems can be evaluated both objectively and subjectively. In this section, we use a synthetic "Grids" color image

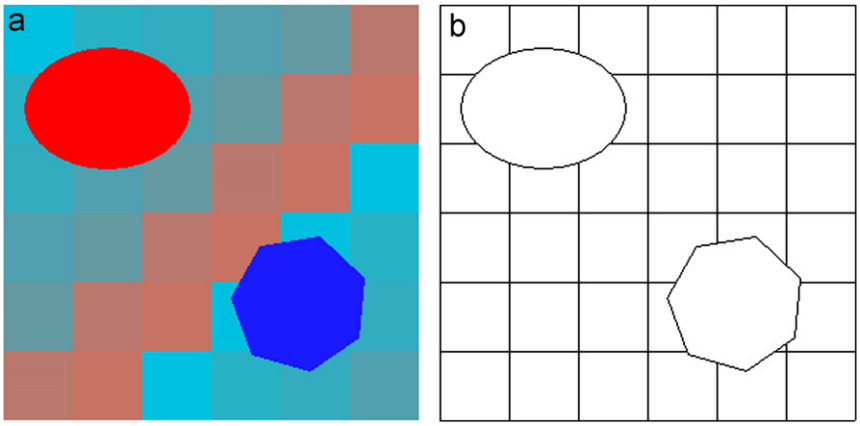

Fig. 1. Synthetic color image "Grids" and the ground truth edge map. (For interpretation of the references to color in this figure legend, the reader is referred to the web version of this article.)

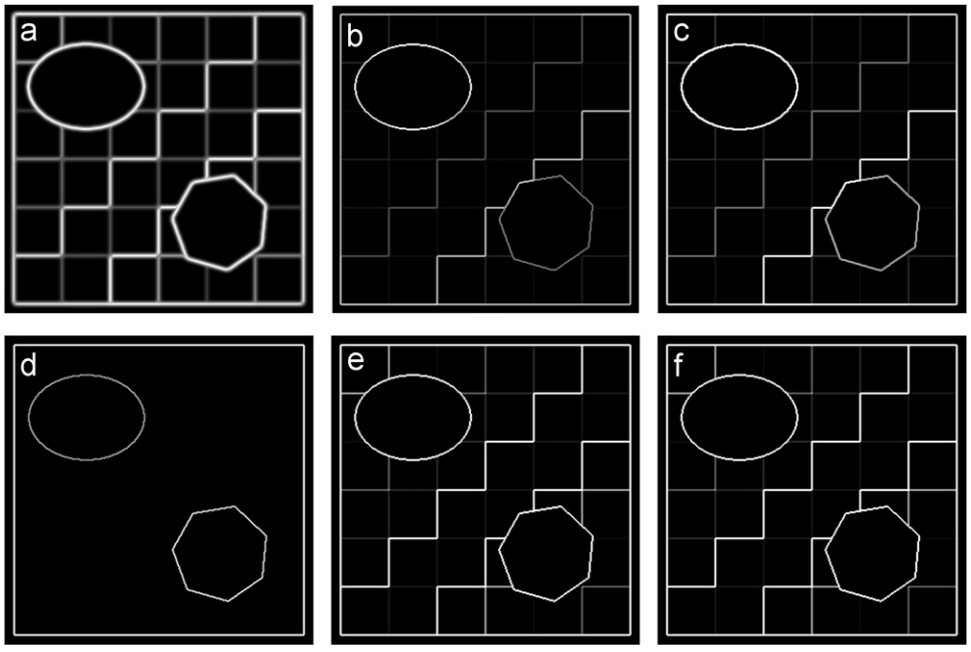

Fig. 2. Gradient magnitudes of "Grids" image produced by various gradient methods: (a) compass operator, (b) RCMG-Median–Mean operator, (c) Scharcanski and Venetsanopoulos' method, (d) luminance-based gradient, (e) Di Zenzo's gradient (θ_+), (f) proposed method.

(Fig. 1) to objectively access the performance of various gradient methods. The test image and the ground truth edge map are generated by a C++ program. To quantify the performance of edge detectors, different criteria have been developed, such as the figure of merit (FOM) [1], precision-recall characteristics (PRC), and receiver operating characteristics (ROC) [39,40]. However, there is no single quantitative evaluation method which is universally accepted by researchers. In this paper, we use the ROC plot, in which the false positive detection rate (**FPR**) is the percentage of the false positive edges to the total true non-edges and the false negative detection rate (**FNR**) is the percentage of the false negative examples to the total true edges. For each gradient operator, the edge map is obtained by adjusting the high and low thresholds of Canny edge detector until the minimum FPR and FNR values are found.

First, we check the accuracy of the gradients produced by various gradient methods: (a) Compass operator, (b) RCMG-Median–Mean operator, (c) Scharcanski and Venetsanopoulos' method, (d) Luminance gradient, (e) Di Zenzo's gradient, and (f) The proposed method. Fig. 2 shows the gradient magnitude images. It can be seen that Compass operator (Fig. 2a) gives thicker and fuzzier edge magnitudes compared to other gradient estimators. The methods including RCMG-Median–Mean operator (Fig. 2b), Scharcanski and Venetsanopoulos' gradient (Fig. 2c), Di Zenzo's vector gradient (Fig. 2e), and the proposed method (Fig. 2f), produce excellent gradient magnitude responses. However, one can observe from the figure that Di Zenzo's gradient operator and the proposed method are more effective in processing the polygon than RCMG-Median–Mean operator. In the gradients obtained from the luminance image (Fig. 2d), only the circle and polygon are detected, whereas all the grid borders in the original image (Fig. 1a) are missing. This is because in the synthetic "Grids" image, the pixels in grids of different colors have the same luminance value (no matter either the lightness mechanism of YUV/YCbCr [23] or the method of channel average is used).

Fig. 3 shows the angle values of the gradients of "Grids" image produced by various gradient methods, where the dark red color denotes that at this position the gradient is undefined (the

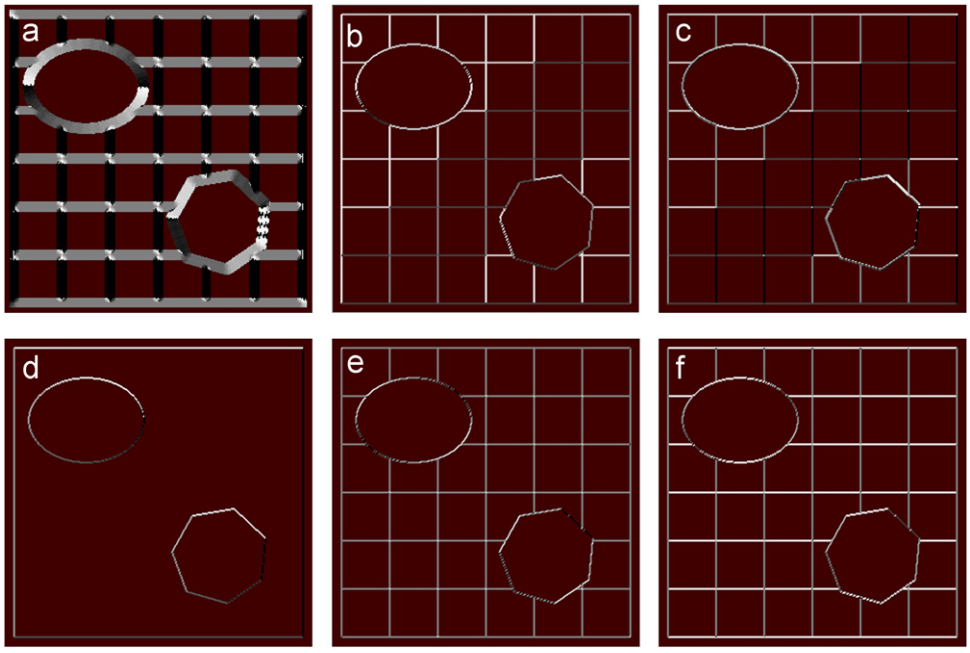

Fig. 3. Gradient directions of "Grids" image produced by various gradient methods that are listed in the same order in the caption of Fig. 2, in which the dark red color denotes that the gradient is undefined (the changes in all directions are the same). The ranges of angle values in (a) to (f) are respectively $[0,\pi]$, $[-\pi,\pi]$, $[0,2\pi]$, $[0,2\pi]$, $[-\pi/2,\pi/2]$, and $[-\pi/2,\pi/2]$.(For interpretation of the references to color in this figure legend, the reader is referred to the web version of this article.)

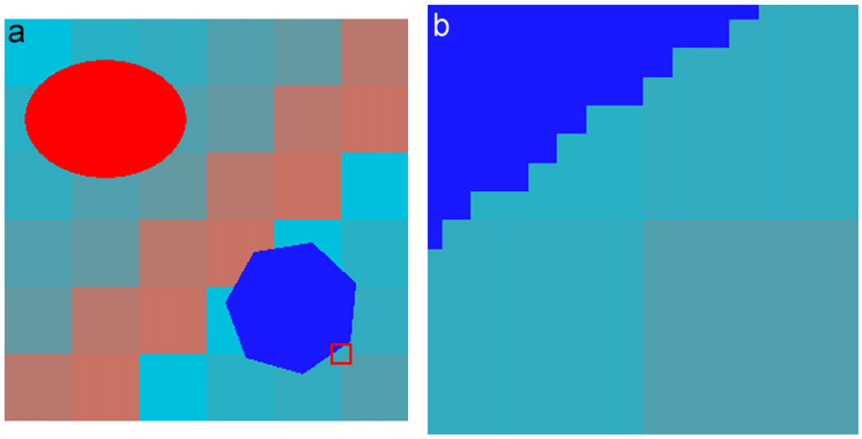

Fig. 4. The marked region used in Fig. 5 for testing the details of gradient directions: (a) red marked region (15×15-pixel), (b) the enlarged image of the red marked region. (For interpretation of the references to color in this figure legend, the reader is referred to the web version of this article.)

changes in all directions are the same). In Fig. 3a to f, gray values 0 and 255 represent 0 and π, $-\pi$ and π, 0 and 2π, 0 and 2π, $-\pi/2$ and $\pi/2$, and $-\pi/2$ and $\pi/2$, respectively. We can see that in Di Zenzo's method (Fig. 3e), the gradient angles of horizontal and vertical edges are the same value 0° (the corresponding gray values are 128). To observe the gradient directions more intuitionally, a 15×15-pixel block is marked at the bottom-right corner in Fig. 4a. Fig. 4b shows the zoomed image of this marked region. Fig. 5 gives the gradient directions of the marked region, which are produced by various gradient methods.

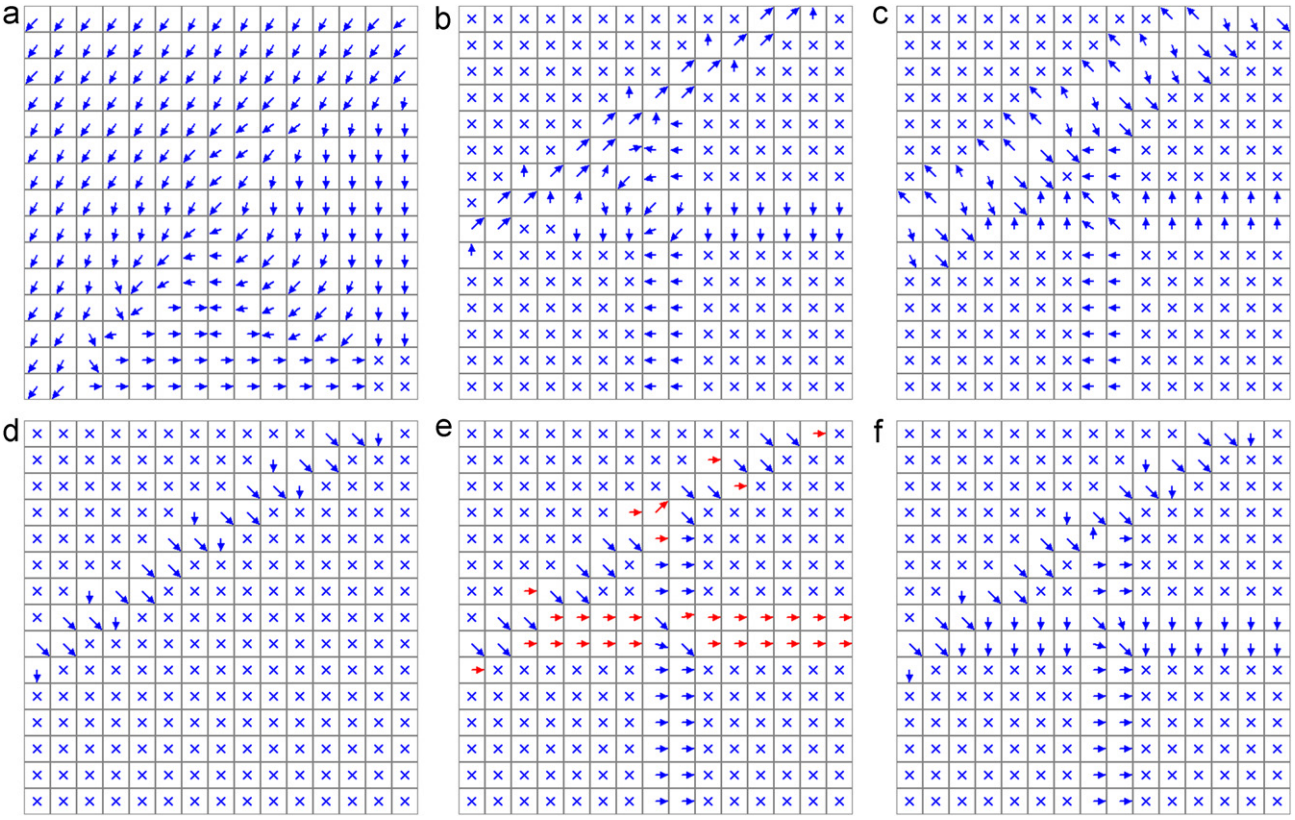

Fig. 5. Gradient directions of the image block marked in Fig. 4(a), produced by various gradient methods that are listed in the same order in the caption of Fig. 2. In the figure, *x* denotes that the gradient is undefined and the red arrow in Fig. 5(e) (Di Zenzo's method) denotes the incorrect gradient (the gradient direction is wrong). (For interpretation of the references to color in this figure legend, the reader is referred to the web version of this article.)

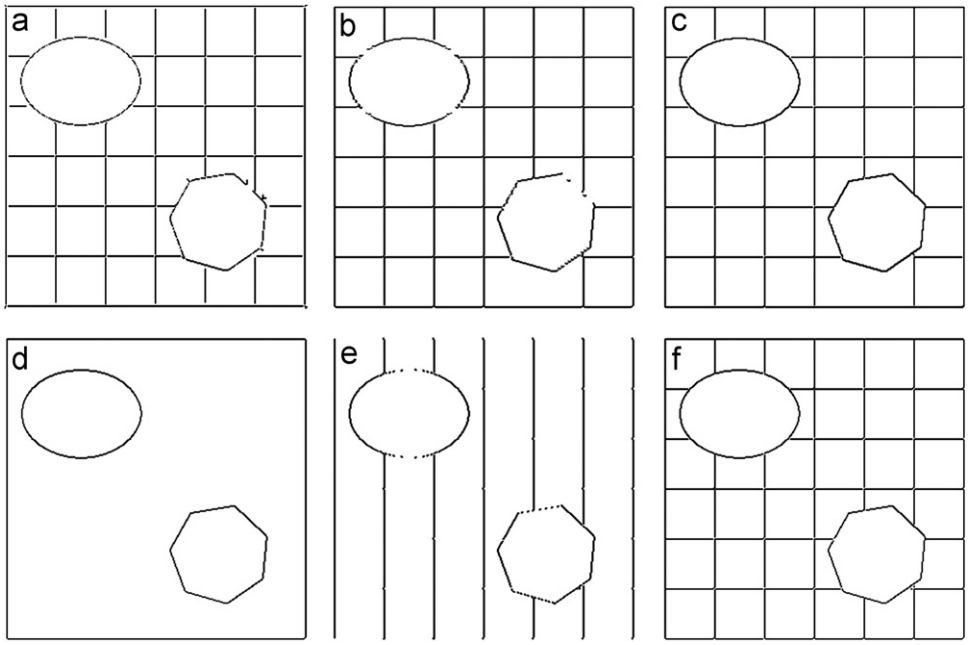

Fig. 6. Edge maps of the synthetic "Grids" image shown in Fig. 1(a), produced by various gradient methods that are listed in the same order in the caption of Fig. 2. The edges are obtained by Canny edge detector, in which the gradients are computed by various gradient methods.

Table 2
False positive detection rates (FPR) and false negative detection rates (FNR) of the "Grids" image, with different distance thresholds τ_d (in pixels). The edge maps are produced by Canny operator in which the gradients are computed by various color gradient estimators.

FPR, FNR Gradien methods	$\tau_d=1$		$\tau_d=3$	
	FPR	FNR	FPR	FNR
Compass	0.000346	0.048996	0.000132	0.043851
RCMG-Median–Mean	0.000071	0.036257	0.000050	0.034542
Scharcanski	0.001983	0.017393	0.001800	0.012984
Luminance	0.000722	0.563939	0.000509	0.558795
Di Zenzo	0.000722	0.433611	0.000509	0.428466
Proposed	0.000632	0.014944	0.000480	0.011514

Table 3
False positive detection rates (FPR) and false negative detection rates (FNR) of the noisy "Grids" images corrupted by mixed noise of p% random impulse noise and white Gaussian noise with mean variance σ (denoted as I p G σ), with different distance thresholds τ_d (in pixels). The edge maps are produced by Canny operator in which the gradients are computed by various color gradient estimators.

FPR, FNR Gradient methods	I1G5				I3G20			
	$\tau_d=1$		$\tau_d=3$		$\tau_d=1$		$\tau_d=3$	
	FPR	FNR	FPR	FNR	FPR	FNR	FPR	FNR
Compass	0.016060	0.055120	0.015663	0.045566	0.014555	0.252817	0.013141	0.218765
RCMG-Median–Mean	0.005625	0.086722	0.004882	0.068839	0.011921	0.335865	0.010558	0.303038
Scharcanski	0.045922	0.143067	0.044437	0.107300	0.021715	0.333660	0.020383	0.301568
Luminance	0.007496	0.557815	0.006591	0.536012	0.019172	0.539196	0.017240	0.492651
Di Zenzo	0.048140	0.167565	0.044407	0.087658	0.040308	0.419157	0.035965	0.314552
Proposed	0.036301	0.127634	0.034449	0.083048	0.039169	0.356198	0.036290	0.286869

Table 4
False positive detection rates (FPR) and false negative detection rates (FNR) of the denoised "Grids" images corrupted by mixed noise of p% random impulse noise and white Gaussian noise with mean variance σ (denoted as $I\ p\ G\ \sigma$), with different distance thresholds τ_d (in pixels). The edge maps are produced by Canny operator in which the gradients are computed by various color gradient estimators.

FPR, FNR Gradient methods	**I1G5 (denoised)**				**I3G20 (denoised)**			
	$\tau_d=1$		$\tau_d=3$		$\tau_d=1$		$\tau_d=3$	
	FPR	FNR	FPR	FNR	FPR	FNR	FPR	FNR
Compass	0.000661	0.059285	0.000173	0.047526	0.005157	0.157521	0.003275	0.112200
RCMG-Median–Mean	0.006672	0.052180	0.006530	0.048751	0.009866	0.183733	0.008717	0.156051
Scharcanski	0.001098	0.029152	0.000814	0.022293	0.005716	0.150906	0.004475	0.121019
Luminance	0.003346	0.561979	0.002848	0.549762	0.001648	0.564919	0.001221	0.554630
Di Zenzo	0.001282	0.205781	0.000264	0.181284	0.004079	0.327536	0.002350	0.285889
Proposed	0.001332	0.027438	0.000987	0.019108	0.004831	0.147967	0.003129	0.106610

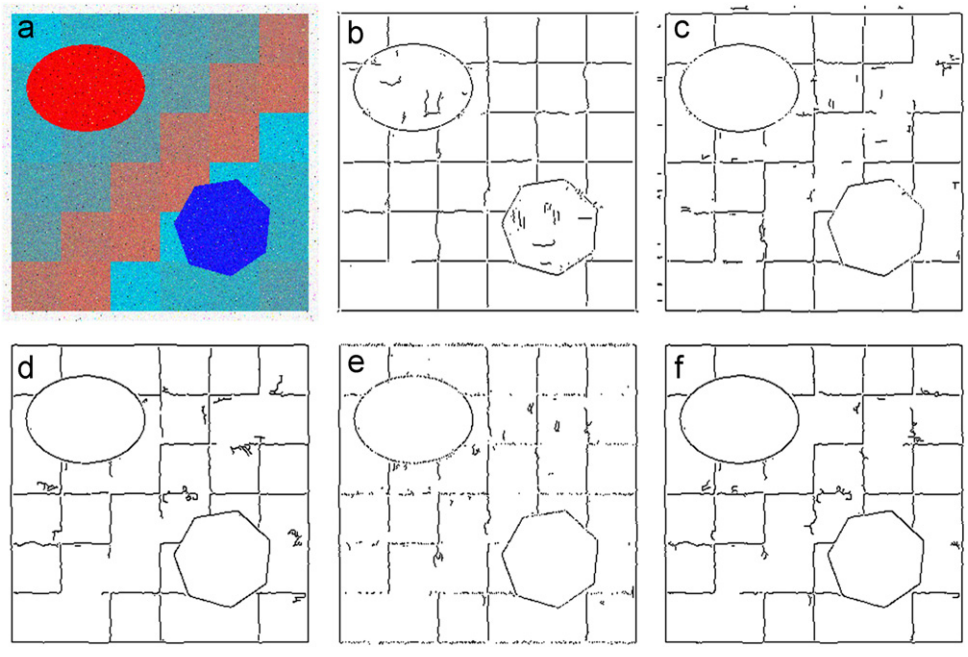

Fig. 7. Edge maps of the denoised "Grids" image produced by various gradient methods: (b) compass operator, (c) RCMG-Median–Mean operator, (d) Scharcanski and Venetsanopoulos' method, (e) Di Zenzo's gradient (θ_+), (f) proposed method. Fig. (a) is the noisy "Grids" image corrupted by mixed noise of 3% random impulse and white Gaussian noise with mean variance 20. The filtered image is obtained by applying the classical vector median filter and the currently-popular BM3D algorithm to the noisy image.

In the figure, x denotes that the gradient is undefined and the red arrow in Fig. 5e (Di Zenzo's method) denotes the incorrect gradient (the gradient direction is wrong). It is obvious that Compass operator (Fig. 5a) produces much thick gradients: many pixels the gradients of which should be undefined are given some valid gradients. The proposed method (Fig. 5f) and Scharcanski and Venetsanopoulos' gradient operator (Fig. 5c) give very good direction estimation, although the latter yields thicker gradients in the bevel edge of the polygon. Careful examination of the figure can find that the directions of the gradients in the polygon bevel edge estimated by Compass operator (Fig. 5a) and RCMG-Median–Mean operator (Fig. 5b) are not correct.

The edge detection results of various gradient methods are presented in Fig. 6. It can be seen from the figure that Di Zenzo's method performs poorly (Fig. 6e), since the horizontal edges are missing. This is consistent with the gradient directions shown in Fig. 3e (the gradient directions of horizontal edges are not correct, as mentioned above). RCMG-Median–Mean operator also works unsatisfactory in detecting the circle and polygon (Fig. 6b). The luminance gradient-based method fails to detect all grid edges (Fig. 6d), since the luminance of pixels in all grids is the same.

Table 2 lists the objective evaluation results of these edge maps in terms of FPR and FNR. τ_d is a pre-defined distance threshold in pixels for judging whether a detection is correct: only when the distance from a detected edge point to the closest true edge is less or

Fig. 8. Two natural images: (a) Parrots (700×512-pixel), (b) Monarch (700×512-pixel). (For interpretation of the references to color in this figure legend, the reader is referred to the web version of this article.)

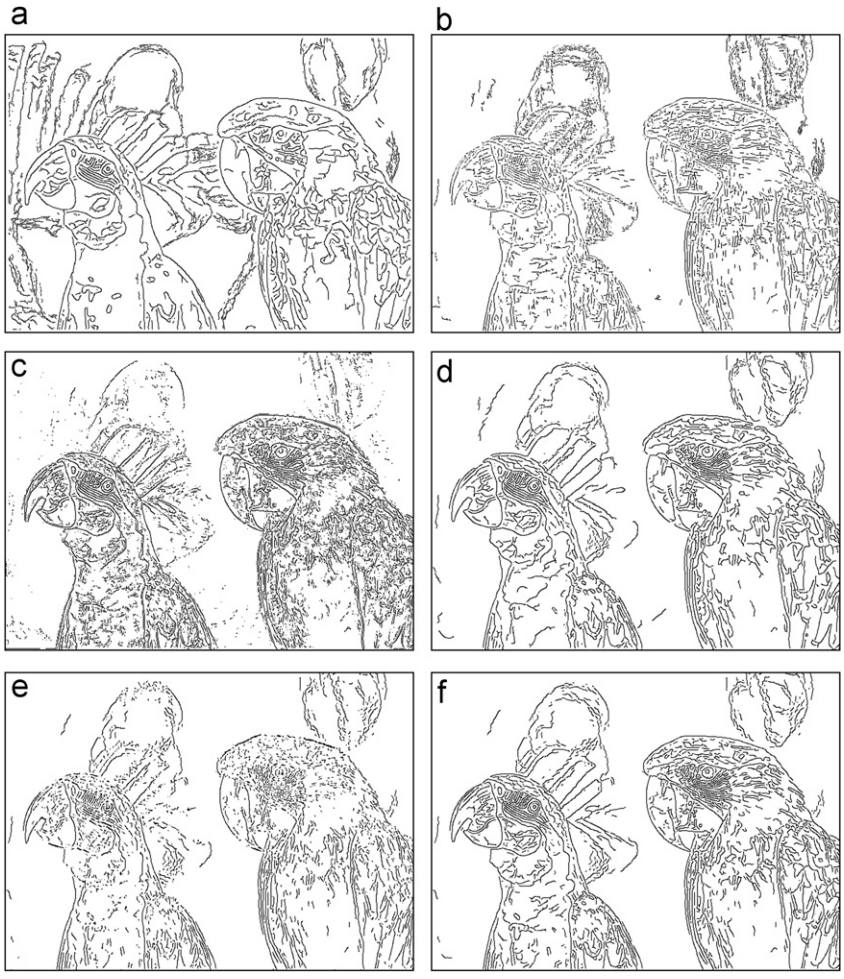

Fig. 9. Edge detection results on natural image "Parrots", produced by various gradient methods that are listed in the same order in the caption of Fig. 2.

equal to τ_d, the detected edge point is regarded as a correct detection. From Table 2, one can notice that RCMG-Median–Mean operator performs better than Compass operator. It seems to be conflict with Fig. 6, since the visual effect of the edge map of Compass operator (Fig. 6a) is more pleasing than that of RCMG-Median–Mean operator (Fig. 6b). This is because many edge points in the circle and polygon detected by Compass operator deviate from the true edges farther compared to RCMG-Median–Mean operator. In summary, according to both the visual effect shown in Fig. 6 and the objective quantitative evaluation given in Table 2, it can be claimed that the improved Di Zenzo's gradient operator outperforms other gradient methods used for the comparison.

Finally, we analyze the performance of the proposed improvement in noisy environments. Since Di Zenzo's gradient operator is based on the squared local contrast variation of multichannel images, both it and the proposed improvement are sensitive to noise. To test the robustness of various gradient methods to noise, we first add two types of mixed noise of color random impulse noise and white Gaussian noise with zero mean value to "Grids" image, and then use various gradient methods to detect edges in noisy images. The color random impulse noise is modeled as channel-related transmission noise [23]. Table 3 lists the FPR and FNR values of various gradient estimators, with different distance thresholds τ_d. It is seen that both Di Zenzo's gradient operator and the proposed improvement perform worse than other methods. However, if a preprocessing is performed before edge detection, the situation is not the same. To verify this, we first use the classical vector median filter [41] (for removing impulse noise) and the currently-popular BM3D algorithm [42] (for suppressing additive Gaussian noise) to filter the noisy images, and then perform Canny edge detection on the denoised images. The quantitative edge detection results are listed in Table 4 and the edge maps are shown in Fig. 7 (the edge map of the luminance gradient-based method is not shown in this figure, since this method fails to detect the edges of all grids). It is easy to observe from the table and figure that, after the preprocessing, the proposed method provides the best edge detection results.

3.2. Natural images

In this section, we evaluate various gradient methods on two natural images by visual inspection. The color test images are "Parrots" (700×512) and "Monarch" (700×512), which are shown in Fig. 8. Similar to the objective evaluation, for each gradient estimator, the edge map is obtained by adjusting the high and low thresholds of Canny edge detector until the best visual effect is attained. Before computing gradients and detecting edges, the two images are pre-smoothed using Gaussian function with mean variance 1.5.

Fig. 9 presents the edge detection results on "Parrots" image. Observation of the edge maps shown in the figure can find that the proposed improvement provides the best visual effect (Fig. 9f). Compass operator (Fig. 9a) and RCMG-Median–Mean operator (Fig. 9b) lose much texture information (notice the vicinity of the eye of right parrot). Compass operator also picks up many trivial edges and fails to detect some important textures and details. Other methods including RCMG-Median–Mean operator produce many

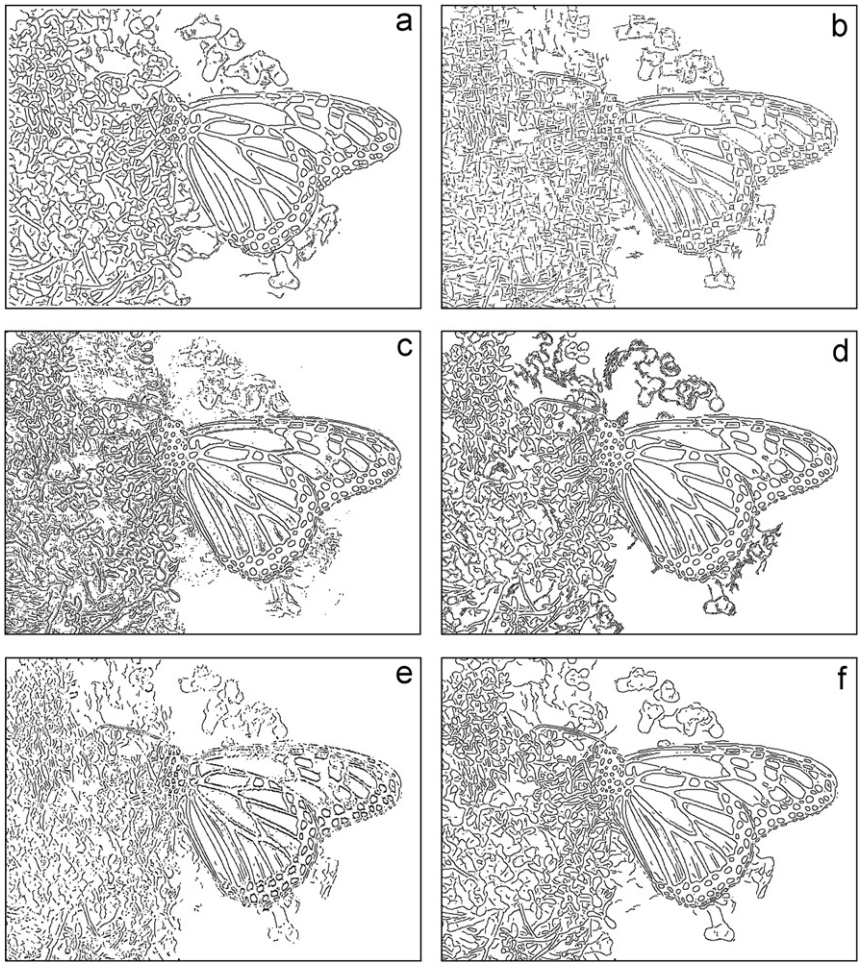

Fig. 10. Edge detection results on natural image "Monarch", produced by various gradient methods that are listed in the same order in the caption of Fig. 2.

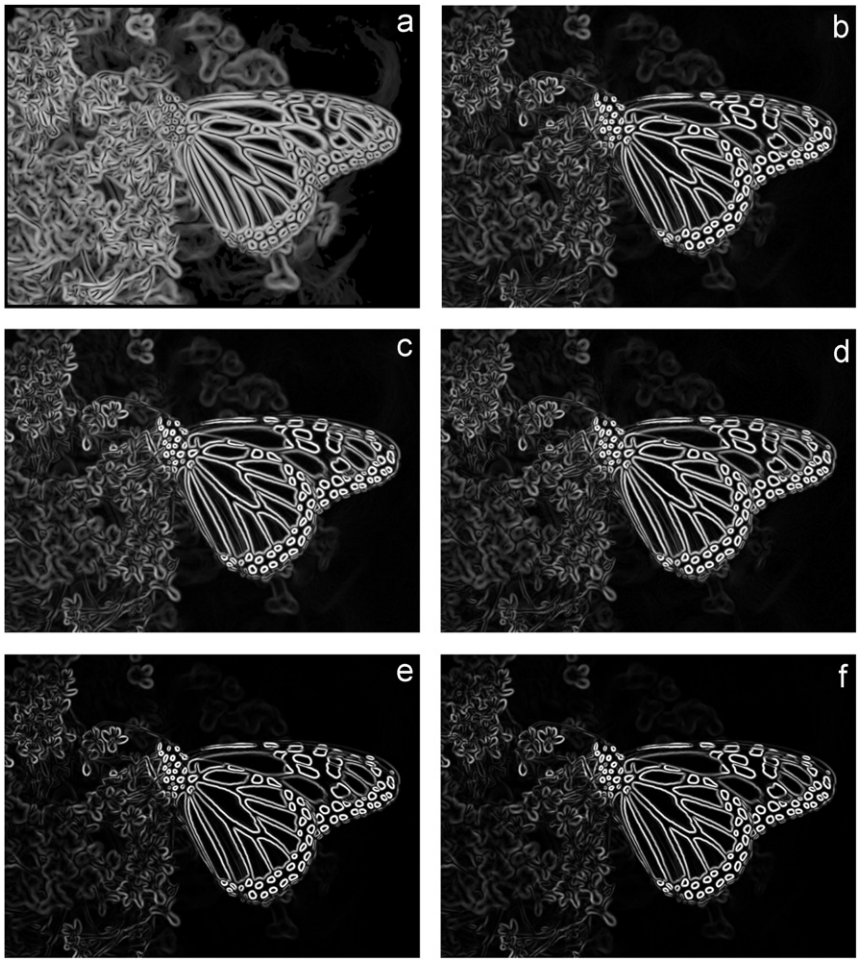

Fig. 11. Gradient magnitude responses of natural image "Monarch", produced by various gradient methods that are listed in the same order in the caption of Fig. 2.

fragmentary edges or discontinuous contours with small line segments. Fig. 10 shows the edge maps of "Monarch" image produced by various gradient methods. Compass operator (Fig. 10a) and the proposed method (Fig. 10f) produce more continuous edges than other methods. Other methods except the luminance gradient-based method (Fig. 10d) yield many dashed dots or very small dashed line segments. Compared to the proposed method, Compass operator and the luminance gradient-based method also produce some dashed dots or fragmentary dashed line segments.

Finally, Fig. 11 shows the unthresholded gradient magnitude responses of "Monarch" image produced by various gradient methods. Examination of this figure can find that Compass operator produces the thickest and fuzziest gradient magnitudes (Fig. 11a). The gradient magnitude images produced by other methods except Di Zenzo's gradient operator (Fig. 11e) and the proposed improvement (Fig. 11f) are also a little fuzzy. The magnitude responses of Di Zenzo's gradient operator and the proposed method are clearer and sharper than those of other gradient estimators, which excellently express the abrupt changes of the color image. However, due to the direction estimation errors, the edge map detected by Di Zenzo's gradient operator is not satisfactory, as shown in Fig. 10e.

4. Conclusions

Estimating gradients of multichannel images is an important issue for multichannel image processing. A currently widely-used gradient method for multichannel images is Di Zenzo's vector gradient operator. However, the uncertainty of Di Zenzo's gradient direction has not well solved to date, which results in errors occurring in many published literature in which Di Zenzo's vector gradient is referenced. In this paper, by analyzing the squared contrast variation function, we obtain the solution to solving the ambiguous problem in Di Zenzo's gradient direction thoroughly. Furthermore, we also analyze the range of gradient direction angle in various cases.

To show the effectiveness of the proposed method, we apply the proposed gradient operator to color edge detection. By replacing the gradients used for non-maximal suppression in grayscale image Canny edge detector with color image gradients, various color versions of Canny edge operator are obtained. The edge detection results are evaluated both quantitatively and qualitatively. The experimental results show that the improved Di Zenzo's gradient operator not only provides more accurate gradient estimation but also is easy to implement and performs fast compared to other state-of-the-art color image gradient methods.

Acknowledgements

This study was supported by the National Natural Science Foundation of China under Grant No. 60972098. The authors would like to thank the reviewers for their valuable comments which help to improve the paper, Dr. Ehsan Nezhadarya for providing the

program for RCMG-Median–Mean gradient operator, and the authors of Compass operator for putting the code on the webpage.

Appendix A. Proof of Theorem 1

Proof. From Eq. (2), we have

$$f(\theta)=\tfrac{1}{2}((E+G)+2F\sin 2\theta+(E-G)\cos 2\theta) \tag{A.1}$$

When $(E-G)^2+F^2=0$, $f(\theta)=1/2(E+G)$, which denotes that the rate of change of the image f(x,y) is invariant to any direction, i.e., it is the same in all directions, so the gradient direction $\theta_{\max}$ in this situation is undefined. Fortunately, studies show that this situation seldom occurs in practical natural images. So in the following we only discuss the case of $(E-G)^2+F^2\neq 0$.

Eq. (A.1) can be written as

$$f(\theta)=\tfrac{1}{2}((E+G)+\sqrt{(E-G)^2+(2F)^2}\cos(2\theta-\varphi)), \tag{A.2}$$

where

$$\begin{cases}\sin\varphi=\frac{2F}{\sqrt{(E-G)^2+(2F)^2}}\\ \cos\varphi=\frac{E-G}{\sqrt{(E-G)^2+(2F)^2}}\end{cases} \tag{A.3}$$

It is easy to conclude from Eq. (A.3) that

$$\varphi\in\begin{cases}[2k\pi,\ 2k\pi+\pi/2], & E-G\geq 0 \text{ and } F\geq 0\\ [2k\pi-\pi/2,\ 2k\pi], & E-G\geq 0 \text{ and } F<0\\ [2k\pi+\pi/2,\ (2k+1)\pi], & E-G<0 \text{ and } F\geq 0\\ [(2k+1)\pi,\ (2k+1)\pi+\pi/2], & E-G<0 \text{ and } F<0\end{cases}, \tag{A.4}$$

Thus, the following equation holds when $(E-G)^2+F^2\neq 0$:

$$\varphi=\mathrm{sgn}(E-G)\arcsin\frac{2F}{\sqrt{(E-G)^2+(2F)^2}}+\begin{cases}2k\pi, & E-G\geq 0\\ (2k+1)\pi, & E-G<0\end{cases} \tag{A.5}$$

To make Eq. (A.2) attain the maximum

$$f_{\max}=\tfrac{1}{2}((E+G)+\sqrt{(E-G)^2+(2F)^2}) \tag{A.6}$$

θ must be equal to $\theta_{\max}$:

$$\theta_{\max}=\tfrac{1}{2}\varphi+k\pi \tag{A.7}$$

According to Eq. (A.5), we have

$$\theta_{\max}=\frac{1}{2}\mathrm{sgn}(E-G)\arcsin\frac{2F}{\sqrt{(E-G)^2+(2F)^2}}+\begin{cases}k\pi, & E-G\geq 0\\ k\pi+\pi/2, & E-G<0\end{cases} \tag{A.8}$$

Combining Eqs. (A.4) and (A.7), the following equation can be obtained

$$\theta_{\max}\in\begin{cases}[k\pi,k\pi+\pi/4], & E-G\geq 0 \text{ and } F\geq 0\\ [k\pi-\pi/4,k\pi], & E-G\geq 0 \text{ and } F<0\\ [k\pi+\pi/4,k\pi+\pi/2], & E-G<0 \text{ and } F\geq 0\\ [k\pi-\pi/2,k\pi-\pi/4], & E-G<0 \text{ and } F<0\end{cases} \tag{A.9}$$

In the following, we discuss Eq. (A.8) according to the sign of the value of $E-G$.When $E-G\geq 0$, from Eqs. (A.9) and (A.8) we have $2\theta_{\max}\in[2k\pi-\pi/2,2k\pi+\pi/2]$ and

$$\sin 2\theta_{\max}=\frac{2F}{\sqrt{(E-G)^2+(2F)^2}}=\frac{2F}{2f_{\max}-E-G} \tag{A.10}$$

So,

$$\cos 2\theta_{\max}=\frac{|E-G|}{\sqrt{(E-G)^2+(2F)^2}}=\frac{E-G}{2f_{\max}-E-G}, \tag{A.11}$$

$$\sin^2\theta_{\max}=\frac{1}{2}(1-\cos 2\theta_{\max})=\frac{f_{\max}-E}{2f_{\max}-E-G} \tag{A.12}$$

Note that $f_{\max}-E=\frac{1}{2}(-(E-G)+\sqrt{(E-G)^2+(2F)^2})\geq 0$ and $2f_{\max}-E-G=\sqrt{(E-G)^2+(2F)^2}>0$ when $(E-G)^2+F^2\neq 0$.

According to Eq. (A.9), $\theta_{\max}\in[k\pi,\ k\pi+\pi/4]$when $E-G\geq 0$ and $F\geq 0$, and $\theta_{\max}\in[k\pi-\pi/4,\ k\pi]$ when $E-G\geq 0$ and $F<0$. So we can obtain from Eq. (A.12) that

$$\theta_{\max}=\arcsin\left(\frac{f_{\max}-E}{2f_{\max}-E-G}\right)^{\pi/2}+k\pi,\ E-G\geq 0 \text{ and } F\geq 0, \tag{A.13}$$

$$\theta_{\max}=-\arcsin\left(\frac{f_{\max}-E}{2f_{\max}-E-G}\right)^{1/2}+k\pi,\ E-G\geq 0 \text{ and } F<0 \tag{A.14}$$

Similarly, when $E-G<0$, according to Eqs. (A.9) and (A.8) we have the following equations:

$2\theta_{\max}\in[(2k+1)\pi-\pi/2,\ (2k+1)\pi+\pi/2]$,

$$\cos 2\theta_{\max}=\frac{-|E-G|}{\sqrt{(E-G)^2+(2F)^2}}=\frac{E-G}{2f_{\max}-E-G}, \tag{A.15}$$

$$\sin^2\theta_{\max}=\frac{1}{2}(1-\cos 2\theta_{\max})=\frac{f_{\max}-E}{2f_{\max}-E-G} \tag{A.16}$$

According Eq. (A.9), $\theta_{\max}\in[k\pi+\pi/4,\ k\pi+\pi/2]$when $E-G<0$ and $F\geq 0$, and $\theta_{\max}\in[k\pi-\pi/2,\ k\pi-\pi/4]$ when $E-G<0$ and $F<0$. So we can obtain from Eq. (A.16) that

$$\theta_{\max}=\arcsin\left(\frac{f_{\max}-E}{2f_{\max}-E-G}\right)^{1/2}+k\pi,\quad E-G<0 \text{ and } F\geq 0, \tag{A.17}$$

$$\theta_{\max}=-\arcsin\left(\frac{f_{\max}-E}{2f_{\max}-E-G}\right)^{1/2}+k\pi,\quad E-G<0 \text{ and } F<0 \tag{A.18}$$

This finishes the proof.

References

[1] W.K. Pratt, Digital Image Processing, third ed., Wiley, New York, 2001.
[2] J.F. Canny, A computational approach to edge detection, IEEE, Transactions on Pattern Analysis and Machine Intelligence 8 (6) (1986) 679–698.
[3] D. Marr, E. Hildreth, Theory of Edge Detection, Proceedings of the Royal Society of London B, Biological Sciences 207 (1167) (1980) 187–217.
[4] R.M. Haralick, Digital step edges from zero crossing of second directional derivatives, IEEE Transactions on Pattern Analysis and Machine Intelligence 6 (1) (1984) 58–68.
[5] O.A. Zuniga, R.M. Haralick, Gradient threshold selection using the facet model, Pattern Recognition 21 (5) (1988) 493–503.
[6] D. Sen, S.K. Pal, Gradient histogram: thresholding in a region of interest for edge detection, Image and Vision Computing 28 (4) (2010) 677–695.
[7] P.R. Hill, C.N. Canagarajah, D.R. Bull, Image segmentation using a texture gradient based watershed transform, IEEE Transactions on Image Processing 12 (12) (2003) 1618–1633.
[8] D. Xiao, W.S. Ng, C.B. Tsang, U.R. Abeyratne, A region and gradient based active contour model and its application in boundary tracking on anal canal ultrasound images, Pattern Recognition 40 (12) (2007) 3522–3539.
[9] X. Zhang, H. Wang, A.W.B. Smith, X. Ling, B.C. Lovell, D. Yang, Corner detection based on gradient correlation matrices of planar curves, Pattern Recognition 43 (4) (2010) 1207–1223.
[10] V.S. Petrovic, C.S. Xydeas, Gradient-based multiresolution image fusion, IEEE Transactions on Image Processing 13 (2) (2004) 228–237.
[11] M. Shi, Y. Fujisawa, T. Wakabayashi, F. Kimura, Handwritten numeral recognition using gradient and curvature of gray scale image, Pattern Recognition 35 (10) (2002) 2051–2059.
[12] L.-L. Huang, A. Shimizu, Y. Hagihara, H. Kobatake, Gradient feature extraction for classification-based face detection, Pattern Recognition 36 (11) (2003) 2501–2511.
[13] D.W. Paglieroni, W.G. Eppler, Resolution analysis for gradient direction matching of object model edges to overhead images, Computer Vision and Image Understanding 113 (2) (2009) 235–248.
[14] R. Machuca, K. Phillips, Applications of vector fields to image processing, IEE, Transactions on Pattern Analysis and Machine Intelligence 5 (3) (1983) 316–329.

[15] M.A. Ruzon, C. Tomasi, Edge, junction, and corner detection using color distributions, IEEE Transactions on Pattern Analysis and Machine Intelligence 23 (11) (2001) 1281–1295.
[16] G. Robinson, Color edge detection, Optical Engineering 16 (5) (1977) 479–484.
[17] S. Di Zenzo, A note on the gradient of a multi-image, Computer Vision, Graphics, and Image Processing 33 (1) (1986) 116–125.
[18] L. Shafarenko, M. Petrou, J. Kittler, Automatic watershed segmentation of randomly textured color images, IEEE Transactions on Image Processing 6 (11) (1997) 1530–1544.
[19] J. Scharcanski, A.N. Venetsanopoulos, Edge detection of color images using directional operators, IEEE Transactions on Circuits and Systems for Video Technology 7 (2) (1997) 397–401.
[20] E. Nezhadarya, R.K. Ward, A new scheme for robust gradient vector estimation in color images, IEEE Transactions on Image Processing 20 (8) (2011) 2211–2220.
[21] A. Cumani, Edge detection in multispectral images, Graphical Models and Image Processing 53 (1) (1991) 40–51.
[22] W. Alshatti, P. Lambert, Using Eigenvectors of a Vector Field for Deriving a Second Directional Derivative Operator for Color Images, in: Proceedings of 5th International Conference on Computer Analysis of Images and Patterns, September 1993, pp. 149–156.
[23] K.N. Plataniotis, A.N. Venetsanopoulos, Color Image Processing and Applications, Springer-Verlag, Berlin, 2000.
[24] A. Koschan, M. Abidi, Detection and classification of edges in color images, IEEE Signal Processing Magazine 22 (1) (2005) 64–73.
[25] S.-Y. Zhu, K.N. Plataniotis, A.N. Venetsanopoulos, Comprehensive analysis of edge detection in color image processing, Optical Engineering 38 (4) (1999) 612–625.
[26] A. Koschan, A comparative study on color edge detection, in: Proceedings of Second Asian Conference on Computer Vision (ACCV), December 1995, vol. 3, pp. 574–578.
[27] S. Wesolkowski, M.E. Jernigan, R.D. Donnie, Comparison of color image edge detectors in multiple color spaces, IEEE International Conference on Image Processing (ICIP) 2 (September 2000) 796–799.
[28] P.E. Trahanias, A.N. Venetsanopoulos, Color edge detection using vector order statistics, IEEE Transactions on Image Processing 2 (2) (1993) 259–264.
[29] P.E. Trahanias, A.N. Venetsanopoulos, Vector order statistics operators as color edge detectors, IEEE Transactions on Systems, Man and Cybernetics, Part B (Cybernetics) 26 (1) (1996) 135–143.
[30] N. Evans, X.U. Liu, A morphological gradient approach to color edge detection, IEEE Transactions on Image Processing 15 (6) (2006) 1454–1463.
[31] A. Shiozaki, Edge extraction using entropy operator, Computer Vision, Graphics, and Image Processing 36 (1) (1986) 1–9.
[32] A. Fotinos, G. Economou, S. Fotopoulos, Use of relative entropy in colour edge detection, Electronics Letters 35 (18) (1999) 1532–1534.
[33] G. Economou, A. Fotinos, S. Makrogiannis, S. Fotopoulos, Color image edge detection based on nonparametric density estimation, IEEE International Conference on Image Processing (ICIP) 1 (2001) 922–925, October.
[34] C. Theoharatos, V. Tsagaris, G. Economou, S. Fotopoulos, V. Anastassopoulos, Edge Detection of Multispectral Images using Nonparametric Local Density Estimation, in: Proceedings of the IASTED International Conference on Signal Processing, Pattern Recognition, and Applications, June 2003, pp. 42–47.
[35] A. Ortiz, G. Oliver, Analysis of colour channel coupling from a physics-based viewpoint: application to colour edge detection, Pattern Recognition 43 (7) (2010) 2507–2520.
[36] S.-C. Cheng, T.-L. Wu, Subpixel edge detection of color images by principal axis analysis and moment-preserving principle, Pattern Recognition 38 (4) (2005) 527–537.
[37] H.-C. Lee, D.R. Cok, Detecting boundaries in a vector field, IEEE Transactions on Signal Processing 39 (5) (1991) 1181–1194.
[38] L. Busin, N. Vandenbroucke, L. Macaire, Color spaces and image segmentation, Advances in Imaging Electron Physics 151 (2008) 65–168.
[39] J. Davis, M. Goadrich, The Relationship Between Precision-Recall and ROC Curves, in: ACM International Conference Proceeding Series, Proceedings of the 23rd International Conference on Machine Learning, June 2006, vol. 148, pp. 233–240.
[40] K. Bowyer, C. Kranenburg, S. Dougherty, Edge detector evaluation using empirical ROC curves, Computer Vision and Image Understanding 84 (1) (2001) 77–103.
[41] J. Astola, P. Haavisto, Y. Neuvo, Vector median filters, Proceedings of the IEEE 78 (4) (1990) 678–689.
[42] K. Dabov, A. Foi, V. Katkovnik, K. Egiazarian, Color image denoising via sparse 3D collaborative filtering with grouping constraint in luminance–chrominance space, in: IEEE International Conference on Image Processing (ICIP), September 2007, vol. 1, pp. 313–316.

Lianghai Jin received the BS and MS degrees in computer science from Central South University (China) in 1988 and Beijing Jiaotong University (China) in 2002, and the PhD degree in pattern recognition and intelligent systems from Huazhong University of Science and Technology (China) in 2008, where he is now an associate professor with the School of Computer Science and Technology. From 1988 to 1999, he was with a railway institute in China as an engineer and senior engineer, respectively. His research interests include color and video image processing.

Hong Liu received the BS and MS degrees in optoelectronic engineering and computer science from Huazhong University of Science and Technology (China) in 1984 and 1995, respectively, and the PhD degree in electronic engineering from Teesside University (United Kingdom) in 2000. She is currently an associate professor with the School of Computer Science and Technology, Huazhong University of Science and Technology. Her research interests include image processing and computer networking.

Xiangyang Xu received the BS, MS, and PhD degrees in computer science from Huazhong University of Science and Technology (China) in 1998, 1991, and 2010, respectively. He is currently an associate professor with the School of Computer Science and Technology, Huazhong University of Science and Technology. His research interests include image processing and analysis.

Enmin Song received the PhD degree in electronic engineering from Teesside University (United Kingdom) in 1999. He is currently a professor with the School of Computer Science and Technology, Huazhong University of Science and Technology, China. His research interests include image processing and algorithm analysis.